Physica D 458 (2024) 133994

Contents lists available at ScienceDirect

Physica D

journal homepage: www.elsevier.com/locate/physd

Transition from traveling to motionless pulses in semiconductor lasers with saturable absorber

F.R. Humire [a,*], K. Alfaro-Bittner [b], M.G. Clerc [c], R.G. Rojas [d]

[a] Departamento de Física, Facultad de Ciencias, Universidad de Tarapacá, Casilla 7-D Arica, Chile
[b] Universidad Rey Juan Carlos, Calle Tulipán s/n, 28933 Móstoles, Madrid, Spain
[c] Departamento de Física and Millennium Institute for Research in Optics, Facultad de Ciencias Físicas y Matemáticas, Universidad de Chile, Casilla 487-3, Santiago, Chile
[d] Instituto de Física, Pontificia Universidad Católica de Valparaíso, Casilla 4059, Valparaíso, Chile

ARTICLE INFO

Communicated by V.M. Perez-Garcia

Keywords:
Nonlinear dynamics
Pulse propagation
Semiconductor lasers with saturable absorber
Symmetry breaking instability

ABSTRACT

Semiconductor lasers show interesting pulse dynamics. We investigate, analytically and numerically, the transition from traveling to motionless pulses in vertical-cavity semiconductor lasers with a saturable absorber. Based on two different approaches, (i) the adiabatic elimination of the charge carriers corresponding to a class A laser and (ii) considering the laser dynamics close to lasing instability (class B lasers), we figure out the relationship between these pulses. The pulses exhibit a continuous transition between traveling to motionless ones. Starting from the asymptotic behavior of the pulse, we are able to set a formula for the pulse speed. In the limit of a small electric field envelope, we elucidate that the observed transition corresponds to the spontaneous breaking instability of reflection symmetry. Employing a reduction method, we set equations for the position, asymmetrical amplitude, and frequency of the pulse. This reduced pulse model shows quite fair agreement with numerical simulations for the different approaches considered for semiconductor lasers with a saturable absorber.

1. Introduction

Spontaneous pulse propagation plays a fundamental role in various biological processes [1–4]. From a physical point of view, pulses correspond to solitary waves, that is, nonlinear waves that propagate without deformation. These pulses are observed in conservative [5–8] or dissipative systems [9–13]. A characteristic of the pulses shape is that they are asymmetric; that is, they do not present symmetry of spatial reflection. Likewise, the pulses speed is constant and determined by the parameters of the system under study. From a dynamics point of view, pulses correspond to homoclinic solutions in the moving reference frame [14]. In the case of conservative systems, the shape and speed propagation of the pulse are determined by the initial condition as a consequence of the translational momentum and energy conservation. This scenario changes completely when one considers dissipative systems. Pulses with the same shape are observed after a transient evolution for different initial conditions. Namely, pulses are attractors with permanent dynamics. The pulse propagation depends on different mechanisms. When connecting two different states, the pulse speed is proportional to the difference of energy [15,16]. However, pulses that connect two equivalent states are also observed, where the most emblematic case are neurons that do not need an electrical potential differential to emit electrical spikes [2–4]. This phenomenon is physically understood because the system is excitable [17–19]. Excitability is an important concept in various fields ranging from geology, biology, chemistry, and physics to nonlinear optics. The latter is based on the fact that the dynamical behavior of the local system has a stable equilibrium (fixed point), which, when it is disturbed, can exhibit a large excursion in the phase space before converging to equilibrium [3]. This behavior is observed in different phase space geometries, for example, near a saddle–node bifurcation, saddle–node on invariant circle bifurcation, and supercritical Andronov–Hopf bifurcation [3]. As one considers the extended coupled system, the pulse solution arises when the amplitude of a perturbation exceeds a critical threshold. Pulses in excitable media have the feature that, once created, a refractory time must pass before creating another pulse. Another mechanism responsible for pulse propagation into two equivalent states is spontaneous spatial reflection symmetry-breaking instabilities in non-variational systems [13,20,21]. This last mechanism is based on the fact that the system does not minimize the free energy. When a non-variational system reaches a stationary equilibrium, it can exhibit permanent dynamics such as oscillatory, chaotic, propagative, and so forth [21–25].

* Corresponding author.
E-mail address: f.humire@academicos.uta.cl (F.R. Humire).

https://doi.org/10.1016/j.physd.2023.133994
Received 28 May 2023; Received in revised form 17 November 2023; Accepted 19 November 2023
Available online 22 November 2023

Semiconductor lasers are ideal for studying pulse dynamics due to their clean detection and potential technological applications [26–32]. The main differences between biological and optical pulses are the significant discrepancies in the scale of the widths and refractory times. In biological cases, they are of the order of 1 ms to 100 ms, while in optical systems, they are of the order of 10 ps to 1 ns. Lasers with a saturable absorber medium with different configurations are excitable devices that present propagative pulses [26,29,31]. Depending on the number of variables involved in the semiconductor laser dynamics, these semiconductor systems are classified as class A or B laser [33,34]. In particular, vertical cavity lasers with intracavity saturable absorbers emit excitable pulses. Since these semiconductor lasers are out of equilibrium and far from primary instability, they exhibit complex, chaotic spatiotemporal dynamical behaviors accompanied by extreme event pulsations [35–37]. However, a complete understanding of the pulse dynamics observed by these optical devices with a broad area is required to envision new applications and perspectives in biological systems.

This work aims to investigate the transition from traveling to motionless pulses in vertical-cavity surface-emitting semiconductor lasers with a saturable absorber. Numerically, we find that semiconductor lasers with saturable absorbers exhibit propagative and static pulses. We consider different approaches: (i) the adiabatic elimination of the charge carriers corresponding to a class A laser and (ii) the laser dynamics close to lasing or oscillatory instability (class B lasers) to understand the relationship between motionless and traveling pulses. In both approaches, the system is not excitable anymore, we can establish that pulses exhibit a continuous (supercritical) transition between traveling to motionless pulses. Starting from the asymptotic behavior of the pulse, we calculate an expression for the pulse speed, which has an excellent agreement with the numerical findings. To shed light on the mechanism of this transition, we consider that the electric field envelope is weak. This approach allows us to elucidate that the observed transition corresponds to the spontaneous breaking instability of reflection symmetry. Based on the reduction method, we deduce a set of equations for the position, asymmetrical amplitude, and global phase of the pulse. This reduced pulse model shows quite fair agreement with numerical simulations for the different approaches considered for semiconductor lasers with a saturable absorber.

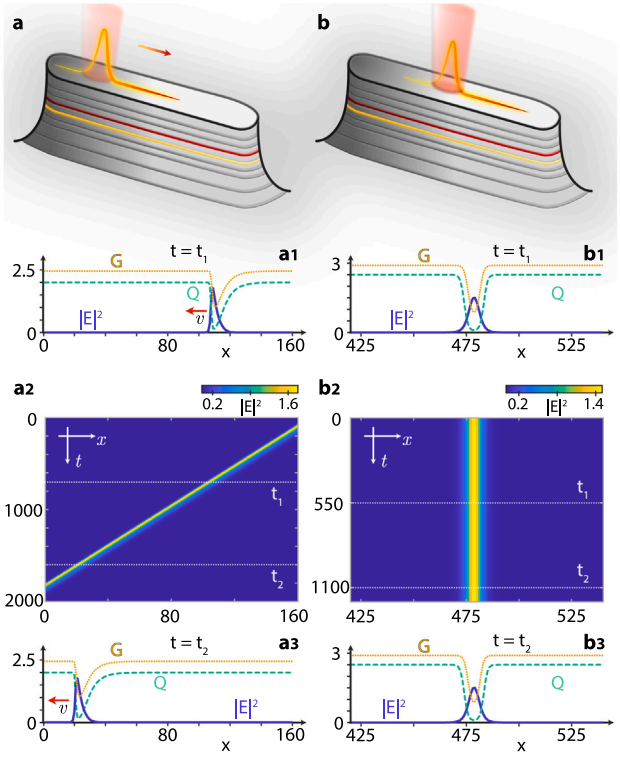

Fig. 1. Pulse dynamics of a vertical-cavity surface-emitting semiconductor lasers with a saturable absorber and broad one-dimensional area model Eq. (1), where left panels show a traveling pulse for $\gamma = 0.07$, $\alpha = 2.0$, $\beta = 0.0$, $A = 2.9$, $B = 2.0$, $s = 10$, and $\Delta t = 0.05$, and right panels show a motionless pulse for $\gamma = 1$, $\alpha = 2.0$, $\beta = 0.0$ $A = 2.9$, $B = 2.5$, $s = 10$, and $\Delta t = 0.05$. Top panels are schematic representations of semiconductor lasers with a saturable absorber with a traveling (a) and a motionless pulse (b). The gray, red, and yellow layers account for the Bragg mirrors, active medium, and saturable absorber, respectively. The lower panels account for the spatiotemporal evolution of a traveling pulse and a motionless one with their respective profiles at different times of the envelope of the electric field intensity $|E|^2$, charge carriers in the active G, and the saturable absorber medium Q.

2. Pulses in semiconductor lasers with saturable absorber

Nonlinear dynamics in semiconductor lasers have been extensively researched owing to their widespread application. Edge-emitting, distributed feedback, and vertical-cavity surface-emitting lasers are examples of class B lasers [33,34]. This is because the polarization of their gain medium can be adiabatically eliminated in Maxwell–Bloch laser equations, leaving only the electric optical field and population inversion as dynamical variables. The vertical-cavity surface-emitting semiconductor laser with an integrated saturable absorber medium is composed of different semiconductor layers that form a sandwich of Bragg mirrors with an active and another saturable absorber medium [38], as illustrated in Fig. 1. Let us consider a semiconductor laser with a saturable absorber with a quasi-one-dimensional geometry. The laser dynamics is described by [35–42]

$$\begin{aligned}
\frac{\partial E}{\partial t} &= [(1-i\alpha)G-(1-i\beta)Q-1]\,E+i\frac{\partial^2 E}{\partial x^2},\\
\frac{\partial G}{\partial t} &= \gamma\left[A-G(1+|E|^2)\right],\\
\frac{\partial Q}{\partial t} &= \gamma\left[B-Q(1+s|E|^2)\right],
\end{aligned} \tag{1}$$

where $E(x,t)$, $G(x,t)$, and $Q(x,t)$ account, respectively, for the envelope of the electric field, the rescaled gain, and the rescaled absorption in the semiconductor laser with a saturable absorber. The factors α and β are standard semiconductor parameters describing phase–amplitude coupling. The last term of the envelope equation stands for the dispersive nearest-neighbor coupling between the lasers, which is of a dispersive nature. γ accounts for non-radiative carrier recombination rates in the gain and absorber media. A and B stand for the pump gain and non-saturable losses. The saturation parameter s in semiconductors is necessarily greater than 1 [31]. Time is rescaled to the cavity photon lifetime, which is the shortest time scale in the system. Note that we have neglected the diffusive transport processes in the charge carriers dynamics G and Q [40]. Models with diffusion in the electrical field envelope have also been under consideration [39–42].

Numerical simulations of the semiconductor laser model equations (1) show traveling pulses because of the excitable nature of the system. These pulse solutions are created by locally altering the electric field with an asymmetrical perturbation; after a transient, the system exhibits a pulse that maintains its shape. Numerical simulations are performed considering finite differences with the Runge–Kutta order-4 algorithm, where Δx and Δt account for the spatial and temporal discretization. In all these simulations, we consider, for simplicity, periodic and null flux boundary conditions. Fig. 1a shows a typical numerical traveling pulse observed in the semiconductor laser with a saturable absorber, model Eq. (1). From these charts, we note that the pulse is asymmetric and that the charge carriers are characterized by exhibiting a refractory tail. The traveling pulses are found for small non-radiative carrier recombination rates γ. When one increases the recombination rate γ, the pulses change their dynamics qualitatively

and are now motionless. Fig. 1b depicts a motionless pulse observed in the semiconductor laser with a saturable absorber model Eq. (1). From these charts, we can infer that the motionless pulse is symmetric. Note that in this region of parameters, considering symmetric or non-symmetric disturbances, the system always ends up with a symmetric motionless pulse after evanescent wave radiation. Hence, the system presents a transition between traveling to motionless pulses when changing the parameters. Notice that supercritical transitions from motionless to traveling pulses were reported in a model for semiconductor lasers where diffusion and dispersion are included as couplings for the electrical envelope in one [39,43] and two spatial dimensions [43,44]. Diffusion is a stabilization mechanism for localized states; in particular, it can be responsible for stabilizing finite-time singularities of localized perturbations [45,46].

Because of the complexity of the semiconductor laser equations (1), we consider different approaches to understand the transitions between traveling to motionless pulses.

2.1. Adiabatic elimination of charge carriers: class A laser

Vertical external-cavity surface-emitting Lasers are class A lasers because the photon lifetime inside the centimeter-long high-finesse external cavity is larger than the carrier lifetime [47–49]. Indeed, the carrier densities can be adiabatically eliminated, leaving only the electric optical field as the dynamical variable [33]. Note that the transition between the class-B and class-A dynamical behaviors of a semiconductor laser has been observed by continuously controlling the lifetime of the photons [50].

Let us consider large non-radiative carrier recombination rates ($\gamma \gg 1$). In this limit, the charge carriers (G and Q) become slave variables of the electric field envelope [51], that is,

$$G[E(x,t)] = \frac{A}{1+|E(x,t)|^2}, \tag{2}$$

$$Q[E(x,t)] = \frac{B}{1+s|E(x,t)|^2}. \tag{3}$$

Using these expressions in the envelope equation of the electric field, one gets (the nonlinear absorber saturable model)

$$\frac{\partial E}{\partial t} = \left(\frac{(1-i\alpha)A}{1+|E|^2} - \frac{(1-i\beta)B}{1+s|E|^2} - 1\right) E + i\frac{\partial^2 E}{\partial x^2}. \tag{4}$$

The above expression corresponds to an amplitude equation with saturable nonlinearity and dispersion coupling. Then, this means that for small and large amplitudes, the system is linear. The envelope $E(x,t) = Re^{i\phi}$ is characterized by two scalar fields, which account for magnitude $R(x,t)$ and argument $\phi(x,t)$ of the envelope. It is important to note that in the large non-radiative carrier recombination rates, the quiescent state, $E = 0$, is no longer excitable. However, the system has a bistable region where one expects to observe pulses [14]. Numerical simulations of the nonlinear saturable model Eq. (4) shows traveling and motionless pulses for different parameters and initial conditions. Fig. 2 illustrates the magnitude (top panels), argument gradient (upper middle panels), and spatiotemporal evolution of the amplitude (lower middle panels) of the observed pulses. Increasing the pump gain A, we observe a supercritical transition between traveling and static solutions. Namely, one observes a continuous transition from traveling to a motionless pulse when changing the pump gain. The lower panels show the bifurcation diagram of the pulse speed v and frequency Ω as a function of the pump gain. Note that the transition for the pulse speed follows a 1/4 power law, that is

$$v = v_0 \sqrt[4]{A_c - A}, \tag{5}$$

where A_c accounts for the critical transition value, $A < A_c$, and v_0 is a dimensional parameter. For $A \geqslant A_c$, the pulse is motionless, i.e., $v = 0$. On the other hand, the pulse frequency also exhibits a supercritical bifurcation but with a critical exponent of 1/2 (see Fig. 2), i.e.,

$$\Omega = \Omega_0 \sqrt{A_c - A}, \tag{6}$$

where Ω_0 is a dimensional parameter.

To characterize the pulse speed v and frequency Ω analytically, we consider the moving reference frame $y \equiv x - vt$ and $\tau \equiv t$ in model Eq. (4), i.e.,

$$\frac{\partial E}{\partial \tau} - v\frac{\partial E}{\partial y} = \left(\frac{(1-i\alpha)A}{1+|E|^2} - \frac{(1-i\beta)B}{1+s|E|^2} - 1\right) E + i\frac{\partial^2 E}{\partial y^2}. \tag{7}$$

Considering the ansatz $E = R(y)\exp\{i(\Omega\tau + \phi(y))\}$, the real and imaginary part of the above equation reads

$$-vR_y = \left[\frac{A}{1+|E|^2} - \frac{B}{1+s|E|^2} - 1\right] R - 2R_y\phi_y - R\phi_{yy}, \tag{8}$$

$$\Omega R - vR\phi_y = \left[-\frac{\alpha A}{1+|E|^2} + \frac{\beta B}{1+s|E|^2}\right] R + R_{yy} - R\phi_y^2. \tag{9}$$

The envelope magnitude of the pulse is characterized by having a bell shape, which asymptotically cancels out on its flanks, $R(y \to \pm\infty) \to 0$, cf. Fig. 2. Likewise, the phase gradient is characterized by tending to a constant on its flanks. Let us respectively call these asymptotic values p_1 and p_2, that is,

$$\partial_y \phi(y) = \begin{cases} p_1, & y \to -\infty, \\ p_2, & y \to \infty. \end{cases} \tag{10}$$

The asymptotic values of the phase gradients depend on the system parameters $p_{\{1,2\}} = p_{\{1,2\}}(A, B, \alpha, \beta, s)$. Using Eq. (9) on its left and right flanks, one obtains the following relations

$$\Omega - p_1 v = (-\alpha A + \beta B) + \left(\frac{A - B - 1}{2p_1 - v}\right)^2 - p_1^2. \tag{11}$$

$$\Omega - p_2 v = (-\alpha A + \beta B) + \left(\frac{A - B - 1}{2p_2 - v}\right)^2 - p_2^2. \tag{12}$$

From these expressions and after straightforward calculations, we obtain the following formulas for the pulse speed and frequency

$$v = p_1 + p_2, \tag{13}$$

$$\Omega = \frac{(A - B - 1)^2 + (p_1 p_2 - (\alpha A - \beta B))(p_1 - p_2)^2}{(p_1 - p_2)^2}. \tag{14}$$

Fig. 3 shows the asymptotic values p_1 and p_2, and the pulse speed v as a function of the pump gain A. Note that this formula has excellent agreement with the numerical results. Since these formulas only use the asymptotic behavior of pulse, we also use them to describe the propagation of the pulses in the semiconductor laser model equation (1). The numerical simulation and the analytical expressions have quite good agreement. Fig. 4 summarizes the comparison between the analytical formula (13) and the numerical results of the semiconductor laser model.

In the next section, we consider another approach, the weak amplitude limit ($E \ll 1$), to shed more light on the supercritical transition between traveling and motionless pulses.

2.2. Weak amplitude limit: class A laser

In the weak limit of the envelope, one expands in the Taylor series the nonlinearities of model Eq. (7), saving the first nonlinearity that saturates the instability of the quiescent state ($E = 0$). Hence, the envelope satisfies (the Ginzburg–Landau equation with diffractive coupling)

$$\frac{\partial E}{\partial t} = \left(\mu + d|E|^2 + \gamma'|E|^4\right) E + i\frac{\partial^2 E}{\partial x^2}, \tag{15}$$

where these parameters are related to the laser ones by $\mu \equiv (A - B - 1) + i(\beta B - \alpha A)$, $d \equiv (Bs - A) + i(\alpha A - \beta Bs)$, and $\gamma' \equiv (A - s^2 B) + i(\beta Bs^2 - \alpha A)$. Considering an amplitude oscillation frame $E(x,t) = E'(x,t)e^{i(\alpha A - \beta Bs)t}$,

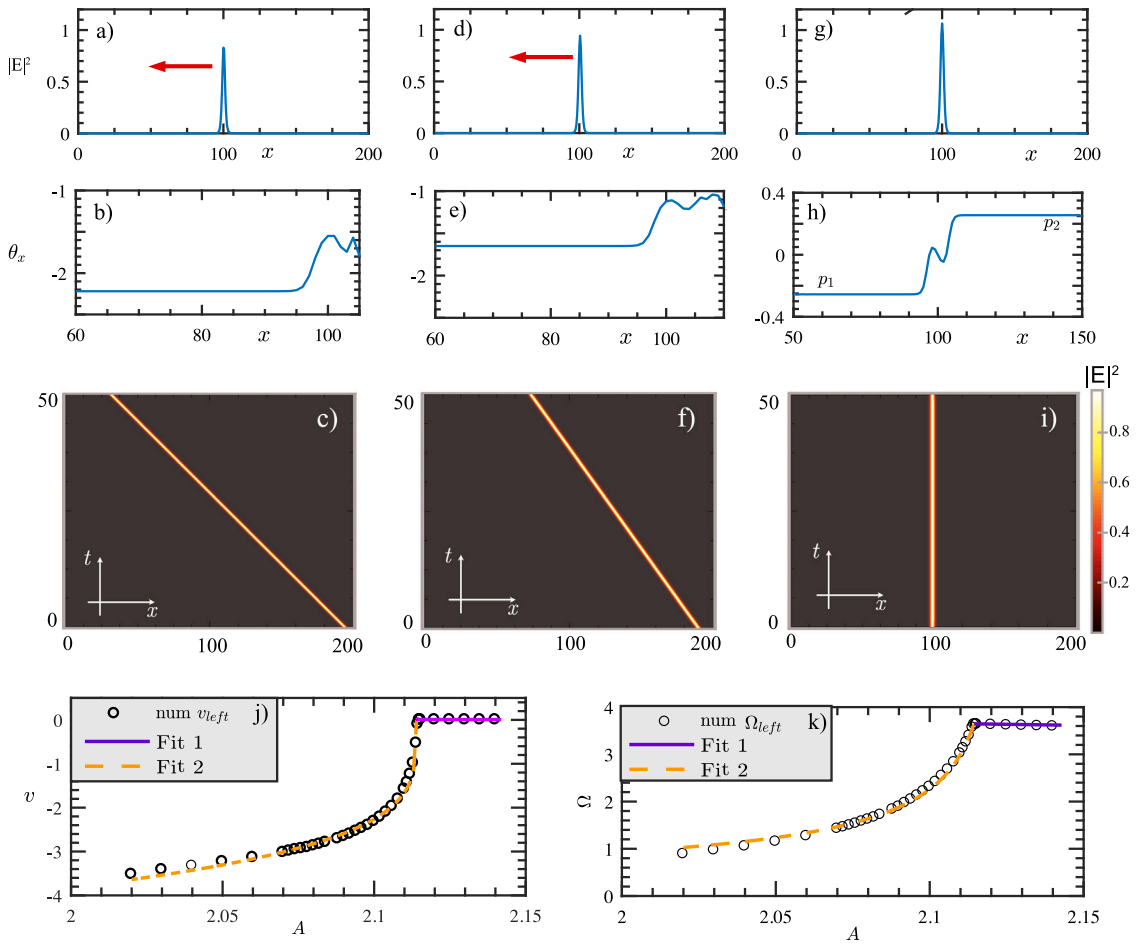

Fig. 2. Pulse dynamics of amplitude equation with saturable nonlinearity and dispersion coupling Eq. (4) for $\alpha = 2.0$, $\beta = -1.3$, $B = 2.0$, $s = 11$, $\Delta x = 0.4$ and $\Delta t = 0.05$. (a) Profile of the intensity of the envelope $|E(x,t)|^2$, (b) profile of the gradient of the argument of the envelope $\phi_x(x,t)$, and (c) spatiotemporal evolution of the magnitude of the envelope of model Eq. (4) with $A = 2.05$. (d) Profile of the envelope intensity $|E(x,t)|^2$, (e) profile of the gradient of the envelope argument $\phi_x(x,t)$, and (f) spatiotemporal evolution of the envelope magnitude of model Eq. (4) with $A = 2.10$, (g) Profile of the envelope intensity $|E(x,t)|^2$, (h) profile of the gradient of the envelope argument $\phi_x(x,t)$, and (i) spatiotemporal evolution of the envelope magnitude with $A = 2.20$, (j) Bifurcation diagram for the pulse speed as a function of pump gain. The circles show the values of the pulse speeds obtained numerically. The orange segmented line is obtained considering the fit $v = v_0\sqrt[4]{A_c - A}$ with $v_0 = -6.571$ and $A_c = 2.114$. (k) Bifurcation diagram for the pulse argument as a function of pump gain. The orange segmented line is obtained considering the fit $\Omega = \Omega_0\sqrt{A_c - A}$ by $\Omega_0 = 0.2975$ and $A_c = 2.114$. The violet curves account for the region where the motionless pulse is observed.

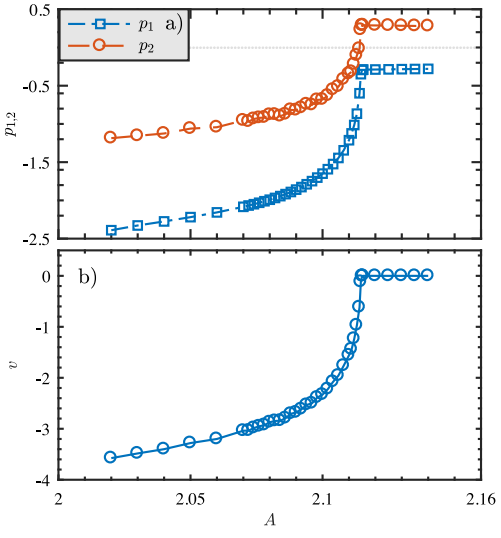

Fig. 3. Characterization of the propagation of pulses in the nonlinear absorber saturable model Eq. (4) by $\alpha = 2.0$, $\beta = -1.3$, $B = 2.0$, and $s = 11$. (a) Asymptotic phase gradient values $p_1 = \partial_y\phi(y \to -\infty)$ and $p_2 = \partial_y\phi(y \to \infty)$ as a function of pump gain A. (b) Pulse speed $v = p_1 + p_2$ as a function of pump gain A.

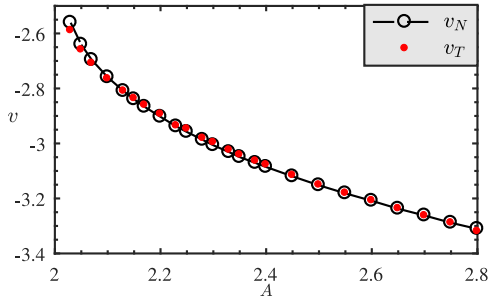

Fig. 4. Characterization of the propagation of pulses in semiconductor lasers with saturable absorber Eq. 1 by $\gamma' = 0.238$, $\alpha = 1.9$, $\beta = 1.8$, $B = 2.0$, and $s = 10$. Pulse speed $v = p_1 + p_2$ as a function of the pump gain A.

the parameter μ is always real. From now on, for the sake of simplicity, we consider that the parameter μ is purely real.

Numerical simulations of the Ginzburg–Landau model Eq. (15) also exhibit traveling and motionless pulse solutions. Fig. 5 shows the profiles and spatiotemporal dynamics of the pulses found in model Eq. (15). In the region of parameters where the traveling pulse solutions exist, and depending on the initial conditions, we observe pulses

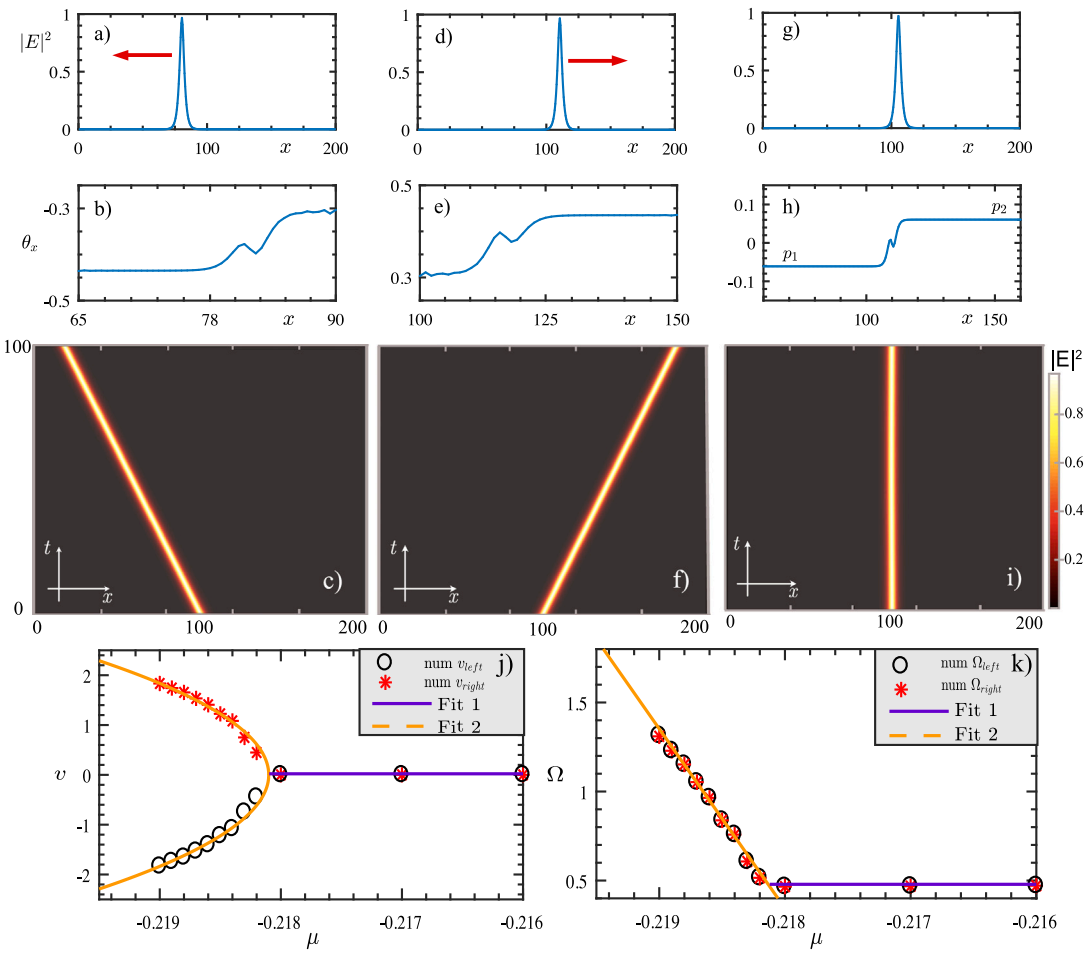

Fig. 5. Transition of traveling to motionless pulse in Ginzburg–Landau model Eq. (15) with $d = 1.1 + i0.7$, $\gamma' = -1 + i = 0.5$, $\Delta x = 0.4$ and $\Delta t = 0.05$. (a), (b), and (c) [(d), (e), (f) and (g), (h), (i)] show the spatiotemporal evolution, respectively, of a traveling pulse towards the left flank, another to the right flank, and a motionless one when $\mu = -0.219$ [$\mu = -0.219$ and $\mu = -0.215$]. (j) Bifurcation diagram of the pulse speed as a function of bifurcation parameter μ. The circles and stars account for the speed of the left and right pulses. The hard orange line is obtained considered the fitting $v = \pm v_1\sqrt{-\mu - \mu_c}$ with $v_1 = 61.22$ and $\mu_c = -0.2181$. (k) Bifurcation diagram of the pulse frequency as a function of bifurcation parameter μ. The circles and stars account for the speed of the left and right pulses. The hard curves stand for the transcritical bifurcation with $\Omega = 1008(\mu_c - \mu) + \Omega_0$ and $\Omega_0 = 0.47$.

that propagate to the left or right flank. Traveling pulses in cubic–quintic Ginzburg–Landau with diffractive coupling was first reported by Sakaguchi [52]. Once again, we observe a continuous transition from traveling to a motionless pulse when modifying a single parameter. Fig. 5 shows the respective bifurcation diagrams as a function of the bifurcation parameter μ. Note that the pulse speed follows a square root type law, that is, $v = v_1\sqrt{\mu_c - \mu}$ with v_1 an adequate dimensional parameter and μ_c is the critical value of the bifurcation parameter; see lower panels of Fig. 5. Additionally, the frequency Ω presents a transcritical bifurcation; that is, the frequency follows a linear power law ($\mu < \mu_c$) and constant $\Omega = \Omega_0$ when $\mu \geqslant \mu_c$, as a function of the bifurcation parameter. Fig. 5 depicts the transition observed for the speed and frequency of the pulse.

Since the pulse speed and frequency formulas [Eqs. (13) and (14)] are calculated in the limit of weak amplitudes, these formulas would also govern the dynamics of the cubic–quintic Ginzburg–Landau equation (15) with diffractive coupling. Fig. 6 compares the results obtained with Eq. (15) and formulas (13) and (14). The system shows excellent agreement with the theoretical formulas and numerical results.

In addition, note that Eq. (15) is invariant to the Galilean-type transformation $E(x,t) = E'(x - ut, t)e^{i\frac{u}{2}(x-u/2t)}$ such that the complex amplitude E' evolves according to

$$\frac{\partial E'}{\partial t'} = \left(\mu + d|E'|^2 + \gamma'|E'|^4\right)E' + i\frac{\partial^2 E'}{\partial x'^2}, \tag{16}$$

where $x' = x - ut$, $t' = t$, and u is the speed of a reference frame with respect to a first frame at rest along the positive direction of the x-axis. Hence, when one changes the inertial reference frame, the solutions become propagative, or their speed changes and the phase is corrected with a linear wave, which propagates with half the velocity of the reference frame. Note that one could identify the reference frame used by measuring the difference between phase and modulus velocity. However, the boundary conditions considered in our work (zero flux or fixed values) break the transformation, and we only observe a solution from the fixed system at the boundary.

3. Analytical characterization of the traveling to motionless pulse transition

To characterize the pulse transition, we use the polar representation of the Ginzburg–Landau equation (15); that is, we introduce the representation $E = R(x,t)e^{i\phi(x,t)}$, where

$$R_t = \left(\mu + \beta_r R^2 + \gamma_r R^4\right)R - 2R_x\phi_x - R\phi_{xx}, \tag{17}$$

$$\phi_t = \left(\beta_i + \gamma_i R^2\right)R^2 + \frac{R_{xx}}{R} - (\phi_x)^2. \tag{18}$$

Note that the complex parameters are decomposed explicitly, that is, $\beta = \beta_r + i\beta_i$, $\gamma' = \gamma_r + i\gamma_i$. For $\mu > \mu_c$, this set of equations has a motionless pulse solution of the form $R(x,t) = R_{sl}(x - x_0)$ and $\phi(x,t) = \Omega t + \phi_{sl}(x - x_0)$ where Ω and x_0 are the oscillation frequency and

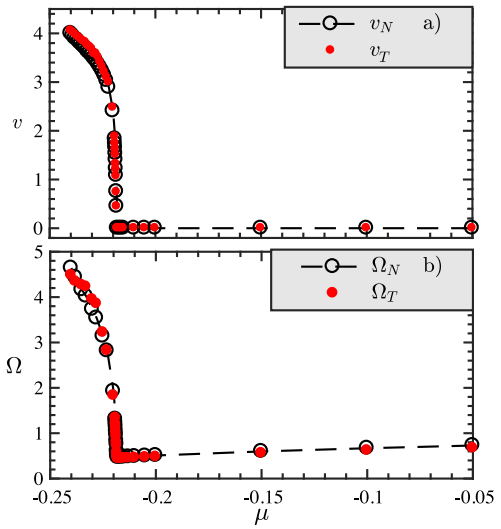

Fig. 6. Comparison of the pulse speed v and frequency Ω for the cubic–quintic Ginzburg–Landau equation (15) with diffractive coupling and analytical formulas (13) and (14). Ginzburg–Landau model was simulated with $d_r = 1.1$, $d_i = 0.7$, $\gamma_r = -1$, $\gamma_i = 0.5$, $\Delta x = 0.4$, and $\Delta t = 0.05$. (a) Pulse speed v as a function of the bifurcation parameter μ. The black circles with stripes and red disks are obtained numerically using the formula (13). (b) Pulse frequency Ω as a function of the bifurcation parameter μ. The black circles with stripes and red disks are obtained numerically using the formula $\Omega = (\mu^2 + p_1 p_2 (p_1 - p_2)^2)/(p_1 - p_2)^2$.

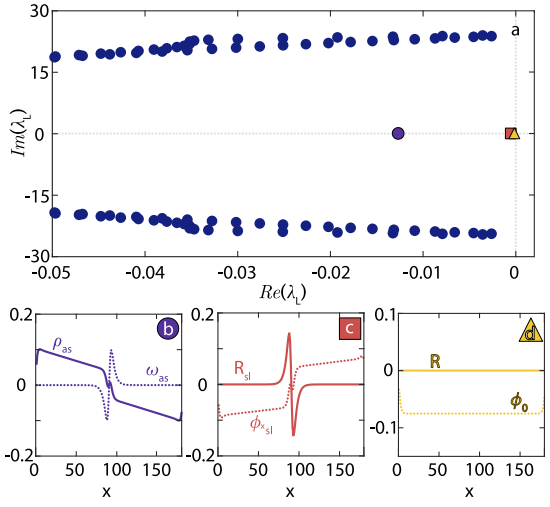

Fig. 7. Numerical stability analysis of the cubic–quintic Ginzburg–Landau equation (15) with diffraction coupling. (a) Numerical spectrum of the cubic–quintic Ginzburg–Landau model Eq. (15) with $\mu = -0.218$, $d_r = 1.1$, $d_i = 0.7$, $\gamma_r = -1$, $\gamma_i = 0.5$ and $\Delta x = 0.4$. The circles, the square, and the triangle account for the eigenvalues of the operator L, formula , obtained numerically. (b), (c), and (d) Eigenfunction of critical modes related to asymmetric mode, spatial, and phase invariance symmetry, respectively. Solid and segmented curves account for the magnitude (R) and phase gradient (ϕ_x) of the eigenfunction.

position of the pulse. x_0 corresponds to the maximum position of $R(x)$. Due to the spatial translation invariance of Eqs. (17) and (18), x_0 is fixed but arbitrary. To study the stability of this solution, we consider a perturbation of the form

$$R = R_{sl}(x - x_0) + \rho(x,t), \tag{19}$$

$$\phi = \Omega t + \phi_{sl}(x - x_0) + \chi(x,t), \tag{20}$$

where the perturbation satisfies the linear equation

$$\begin{pmatrix} \partial_t \rho \\ \partial_t \phi \end{pmatrix} = L \begin{pmatrix} \rho \\ \chi \end{pmatrix}, \tag{21}$$

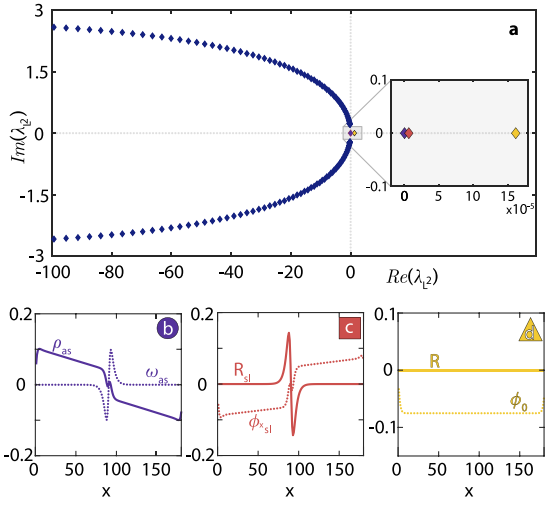

Fig. 8. (a) Numerical spectrum of L^2 with $\mu = -0.218$, $d_r = 1.1$, $d_i = 0.7$, $\gamma_r = -1$, $\gamma_i = 0.5$, and $\Delta x = 0.4$. The circles, the square, and the triangle account for the eigenvalues of the operator L^2 obtained numerically. (b), (c), and (d) Eigenfunction of critical modes related to asymmetric mode, spatial, and phase invariance symmetry, respectively. Solid and segmented curves account for the magnitude (R) and phase gradient (ϕ_x) of the eigenfunction.

and the linear operator L has the form

$$L = \begin{pmatrix} f(R_{ls}) - \phi_{ls,xx} - 2\phi_{ls,x}\partial_x, & -R_{ls}\partial_{xx} - 2R_{ls,x}\partial_x \\ 2d_i R_{ls} + 4\gamma_i R_{ls}^3 + \frac{\partial_{xx}}{R_{ls}} - \frac{\partial_{xx} R_{ls}}{R_{ls^2}} & -2\phi_{ls,x}\partial_x \end{pmatrix}, \tag{22}$$

with $f(R_{ls}) \equiv \mu + 3d_r R_{ls}^2 - 5\gamma_r R_{ls}^4$. Due to the complexity of the linear operator, an analytical analysis is difficult to access. Then, we numerically calculate the eigenvalues and eigenvectors near the critical point of the transition between traveling to motionless pulse. Fig. 7a shows the spectrum (eigenvalue set) obtained numerically for this linear operator. Note that due to the invariance of spatial ($x \to x + x'$) and phase ($\phi \to \phi + \phi_0$) translation, the system has two eigenvalues at the origin of the complex plane. These two Goldstone modes are, respectively, represented by the orange square (spatial translation) and yellow triangle (phase invariance). Observe that, as expected, the mode associated with the translation corresponds to the spatial derivative of the pulse solution (see Fig. 7c), and the phase mode corresponds to the constant eigenvector (see Fig. 7d). By changing the bifurcation parameter μ, we observe that an eigenvalue (purple disk) approaches the origin of the complex plane. This is a manifestation of the emergence of motionless pulse instability. Fig. 7b shows the eigenvector associated with the mode that causes the instability. It is important to note that this mode is spatially asymmetric. Therefore, the transition from traveling to motionless pulses corresponds to a spontaneous reflection breaking symmetry.

When the bifurcation parameter μ approaches the critical parameter μ_c, the eigenvalue of the asymmetric mode collides with the origin in the complex plane; the eigenvector merges with the translation mode. Therefore, the instability is characterized by three eigenvalues at the origin of the complex plane with multiplicity equal to two (two linearly independent eigenvectors). In Arnold's notation, these instabilities correspond to 0^20 bifurcation [53]. This type of instability is expected to exhibit chaotic behavior similar to the Lorenz model [54,55]. To characterize this instability, one can use the strategy based on the Jordan decomposition; that is, one must calculate the spectrum of L^2, which allows us to obtain three independent critical eigenvectors. Fig. 8 shows the spectrum of the operator L^2 and its respective critical modes. Notice the eigenvectors satisfy the following properties for the translation mode

$$L \begin{pmatrix} \partial_x R_{sl}(x) \\ \partial_x \phi_{sl}(x) \end{pmatrix} = \begin{pmatrix} 0 \\ 0 \end{pmatrix}, \tag{23}$$

the phase mode

$$L\begin{pmatrix}0\\ \phi_0\end{pmatrix}=\begin{pmatrix}0\\ 0\end{pmatrix}, \tag{24}$$

and the critical asymmetrical mode

$$L\begin{pmatrix}\rho_{as}(x)\\ \omega_{as}(x)\end{pmatrix}=\begin{pmatrix}\partial_x R_{sl}(x)\\ \partial_x \phi_{sl}(x)\end{pmatrix}. \tag{25}$$

Hence, this last critical mode is an eigenvector of L^2, that is,

$$L^2\begin{pmatrix}\rho_{as}(x)\\ \omega_{as}(x)\end{pmatrix}=\begin{pmatrix}0\\ 0\end{pmatrix}. \tag{26}$$

This eigenvector is the only one that is not analytically accessible, so it is only determined numerically.

Starting from the eigenvectors and following a similar strategy to characterize the transition between traveling to stationary pulses [21], we consider the ansatz

$$\begin{pmatrix}R\\ \phi\end{pmatrix}=\begin{pmatrix}R_{sl}[x-x_0(\epsilon t)]\\ \Omega t+\phi_{sl}[x-x_0(\epsilon t)]\end{pmatrix}+\epsilon\chi(\epsilon^2 t)\begin{pmatrix}\rho_{as}(x-x_0)\\ \omega_{as}(x-x_0)\end{pmatrix}+\begin{pmatrix}0\\ \phi_0(\epsilon^2 t)\end{pmatrix}+\epsilon^3\begin{pmatrix}P(x,x_0,\chi)\\ \Theta(x,x_0,\chi)\end{pmatrix}. \tag{27}$$

The first vector of the right-hand side accounts for the motionless pulse solution. The pulse position $x_0(\epsilon t)$ and phase $\phi_0(\epsilon^2 t)$ have been promoted to temporal functions that account for the pulse dynamics. Note that these variables have a slow dynamic characterized by the small control parameter ϵ, which in turn accounts for the order of the bifurcation parameter ($\epsilon\sim\sqrt{\mu_c-\mu}$). $\chi(\epsilon^2 t)$ stands for the amplitude of the asymmetrical critical mode. The third vector on the right-hand side represents the phase mode. Finally, the last term accounts for the nonlinear corrections in χ.

Introducing the previous ansatz in the cubic–quintic Ginzburg–Landau equation (15) with diffractive coupling and considering the linear equation in the perturbations P and Θ, we get

$$\epsilon^3 L\begin{pmatrix}P\\ \Theta\end{pmatrix}=\begin{pmatrix}-\epsilon\dot{x}_0\partial_z R_{ls}+\epsilon^2\chi\dot{x}_0\partial_z\rho_{as}+\epsilon^3\dot{\chi}\rho_{as}\\ \epsilon\dot{x}_0\partial_z\phi_{ls}+\epsilon^2(\dot{\phi}_0-\chi\dot{x}_0\partial_z\omega_{ls})-\epsilon^3\dot{\chi}\omega_{ls}\end{pmatrix}+\begin{pmatrix}H_1\\ H2\end{pmatrix} \tag{28}$$

where

$$\begin{aligned}H_1 &= -d_r(\epsilon^3\chi^3\rho_{as}^3+3\epsilon^2 R_{ls}\chi^2\rho_{as}^2+3\epsilon\chi R_{ls}^2\rho_{ls}^2\rho_{as})\\ &+\gamma_r(10\epsilon^3\chi^3\rho^3R_{ls}^2+10\epsilon^2\chi^2\rho_{as}^2R_{ls}^3+5\epsilon\chi\rho_{as}R_{ls}^4)\\ &+\epsilon\chi\rho_{as}\partial_{zz}\phi_{rl}+\epsilon^2\chi^2\rho_{as}\partial_{zz}\omega_{as}+2\epsilon\chi\partial_z\phi_{rl}\partial_z\rho_{as}\\ &+2\epsilon\chi\partial_z\omega_{as}\partial_z R_{ls}+2\epsilon^2\chi^2\partial_z\omega_{as}\partial_z\rho_{as}\\ &+\epsilon\chi R_{ls}\partial_{zz}\omega_{as}-\mu_r\epsilon\chi\rho_{as},\end{aligned} \tag{29}$$

$$\begin{aligned}H_2 &= -d_i(\epsilon^2\chi^2\rho_{as}^2+2\epsilon\chi R_{ls}\rho_{as})\\ &-\gamma_i(4\epsilon^3\chi^3\rho_{as}^3R_{ls}+6\epsilon^2\chi^2\rho_{as}^2R_{ls}^2+4\epsilon\chi\rho_{as}R_{ls}^3)\\ &-2\epsilon\chi\partial_z\omega_{as}\partial_z\phi_{ls}-\epsilon^2\chi^2(\partial_z\omega_{as})^2\\ &+\frac{\epsilon\chi}{R_{ls}}\partial_{zz}\rho_{as}+\frac{\epsilon\chi}{R_{ls}^2}\rho_{as}\partial_{zz}R_{ls}+\frac{\epsilon^2\chi^2}{R_{ls}^2}\rho_{as}\partial_{zz}\rho_{as},\end{aligned} \tag{30}$$

and $\mu_r=\mu_c+\epsilon^2\Delta\mu$.

To solve this linear equation (28), we use the Fredholm alternative [56]. Thus, we introduce the inner product

$$\langle\vec{f}(x)|\vec{g}(x)\rangle=\int_{-\infty}^{\infty}\vec{f}\cdot\vec{g}\,dx, \tag{31}$$

which allows us to define and calculate the adjoint operator $L^\dagger$, i.e., $\langle L^\dagger\vec{f}(x)|\vec{g}(x)\rangle\equiv\langle\vec{f}(x)|L\vec{g}(x)\rangle$. We have numerically calculated the spectrum of the adjoint operator $L^\dagger$. Fig. 9 shows the spectrum of this operator and its critical eigenvectors. Then, the linear equation (28) has a solution if the right-hand side of this linear equation is orthogonal to the elements of the kernel of $L^\dagger$ [56]. Operator $L^\dagger$ has three critical vectors near the transition depicted by the lower panels shown in Fig. 9. We obtain three equations by applying the solvability condition or Fredholm alternative for each critical eigenvector. We get the following

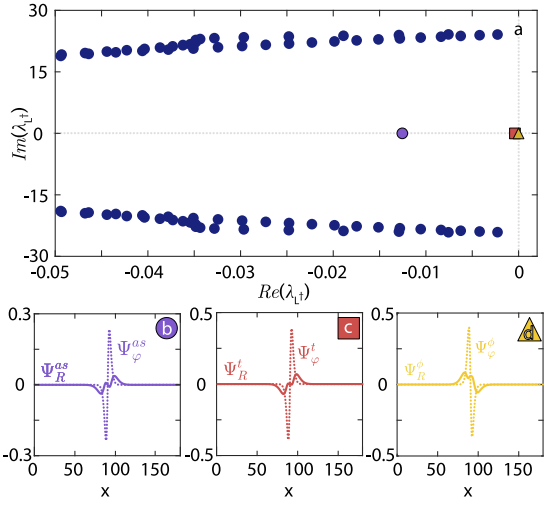

Fig. 9. Numerical spectrum of the adjoint operator $L^\dagger$ with $\mu=-0.218$, $d_r=1.1$, $d_i=0.7$, $\gamma_r=-1$, $\gamma_i=0.5$, and $\Delta x=0.4$. The circles, the square, and the triangle are only the eigenvalues obtained numerically. The purple circle, the red square, and the yellow triangle are the critical values. The lower panels show the respective eigenfunctions of the critical elements.

equations using the symmetry properties of the eigenvectors, and after straightforward calculations (reduced pulse dynamics)

$$\dot{\chi} = g\chi+f\chi^3, \tag{32}$$

$$\dot{x}_0 = a\chi, \tag{33}$$

$$\dot{\phi}_0 = b\chi^2, \tag{34}$$

where

$$f = \frac{d_r\langle\psi_R^{as}|\rho_{as}^3\rangle+5\langle\psi_R^{as}|R_{ls}^2\rho_{as}\rangle+4\gamma_i\langle\psi_\varphi^{as}|R_{ls}\rho_{as}^2\rangle}{\langle\psi_R^{as}|\rho_{as}\rangle+\langle\psi_\varphi^{as}|\omega_{as}\rangle}-\frac{1}{6}\frac{\langle\psi_\varphi^{as}|\frac{\partial_{xx}R_{ls}}{R_{ls}^4}\rho_{as}^2\rangle}{\langle\psi_R^{as}|\rho_{as}\rangle+\langle\psi_\varphi^{as}|\omega_{as}\rangle}, \tag{35}$$

$$g = \frac{\langle\psi_R^{as}|\rho_{as}\rangle}{\langle\psi_R^{as}|\rho_{as}\rangle+\langle\psi_\varphi^{as}|\omega_{as}\rangle}\Delta\mu, \tag{36}$$

$$\begin{aligned}a &= \frac{2d_i\langle\psi_\varphi^t|R_{ls}\rho_{as}\rangle+4\gamma_i\langle\psi_\varphi^t|R_{ls}^3\rho_{as}\rangle+\langle\psi_\varphi^t|\frac{\partial_{xx}\rho_{as}}{R_{ls}}\rangle}{\langle\psi_\varphi^t|\partial_x\phi_{ls}\rangle+\langle\psi_R^t|\partial_x R_{ls}\rangle}\\ &+\frac{\mu\langle\psi_R^t|\rho_{as}\rangle-\langle\psi_\varphi^t|\frac{\partial_{xx}R_{ls}}{R_{ls}^2}\rho_{as}\rangle+3d_r\langle\psi_R^t|R_{ls}^2\rho_{as}\rangle}{\langle\psi_\varphi^t|\partial_x\phi_{ls}\rangle+\langle\psi_R^t|\partial_x R_{ls}\rangle}\\ &-\frac{\langle\psi_R^t|\partial_{xx}\omega_{as}R_{ls}\rangle+\langle\psi_R^t|\partial_{xx}\phi_{ls}\rho_{as}\rangle+2\langle\psi_R^t|\partial_x\omega_{as}\partial_x R_{ls}\rangle}{\langle\psi_R^t|\partial_x\phi_{ls}\rangle+\langle\psi_R^t|\partial_x R_{ls}\rangle}\\ &-\frac{5\gamma_r\langle\psi_R^t|\rho_{as}R_{ls}^4\rangle}{\langle\psi_\varphi^t|\partial_x\phi_{ls}\rangle+\langle\psi_R^t|\partial_x R_{ls}\rangle},\end{aligned} \tag{37}$$

$$\begin{aligned}b &= \frac{3d_r\langle\psi_R^\varphi|R_{ls}\rho_{as}^2\rangle-\langle\psi_R^\varphi|\partial_{xx}\omega_{ls}\rho_{as}\rangle-2\langle\psi_R^\varphi|\partial_x\omega_{as}\partial_x\rho_{as}\rangle}{\langle\psi_\varphi^\varphi|1\rangle}\\ &+\frac{d_i\langle\psi_\varphi^\varphi|\rho_{as}^2\rangle+6\gamma_i\langle\psi_\varphi^\varphi|R_{ls}^2\rho_{as}^2\rangle+\frac{1}{2}\langle\psi_\varphi^\varphi|\frac{\partial_{xx}R_{ls}}{R_{ls}^3}\rho_{as}^2\rangle}{\langle\psi_\varphi^\varphi|1\rangle}\\ &+\frac{2\langle\psi_\varphi^\varphi|(\partial_x\omega_{as})^2\rangle-c\langle\psi_R^\varphi|\partial_x\rho_{as}\rangle+c\langle\psi_\varphi^\varphi|\partial_x\omega_{as}\rangle}{\langle\psi_\varphi^\varphi|1\rangle}.\end{aligned} \tag{38}$$

It is important to note that the coefficient g is proportional to the bifurcation parameter $\Delta\mu$, which order is ϵ^2. When numerically evaluating the coefficient f, we find that it is negative and of order 0.01.

Eq. (32) shows that the system has a pitchfork bifurcation for the asymmetric mode; for positive μ, depending on the initial condition, χ

acquires a positive or negative value of the form $\chi = \sqrt{g/|f|} \sim \Delta\mu^{1/2}$, which is consistent with the numerical observations illustrated in Fig. 5. We infer from Eq. (33) that the pulse velocity $v = \dot{x}_0$ is proportional to the asymmetric mode amplitude χ, that is, $v \sim \chi \sim \Delta\mu^{1/2}$, see Fig. 5. So, the speed increases with the square root of the bifurcation parameter. Hence, if the mode has a positive (negative) amplitude, the pulse propagates to the right (left) flank. Formula (34) tells us how the traveling pulse oscillation frequency $\Omega + \dot{\phi}_0$ is adjusted, which is proportional to the square of the asymmetric mode amplitude, i.e., $\Omega + \dot{\phi}_0 \sim \Omega + \Delta\mu$. Then, the frequency increases linearly with the bifurcation parameter, as shown in Fig. 5.

We have numerically evaluated the coefficients of the reduced pulse dynamics model and compared this description with numerical simulations of the Ginzburg–Landau cubic–quintic equation with diffractive coupling finding a good agreement. Fig. 10 summarizes this comparison.

Note that a similar reduced method has been used by one of our authors to characterize the transition from motionless to traveling localized structures in a scalar prototype model of pattern formation [21]. The central manifold that characterizes the dynamics of this transition is composed of the position of the localized structure and the amplitude of the asymmetric mode that produces the spontaneous symmetry breaking. Hence, the transition of these localized structures is described by a model similar to the set of Eqs. (32) and (33). Likewise, transitions between stationary and traveling fronts in parametrically driven systems have been described using the same strategy and obtaining a similar set of equations for the front position and asymmetric modes [23,24].

3.1. Beyond the supercritical transition

As one moves away from the transition from traveling to static pulses, one observes that the dynamical behavior is no longer described by the reduced model (see Fig. 10). To account for the change in the behavior of the speed and frequency of the pulse away from the bifurcation point, we consider the following ansatz

$$\begin{pmatrix} R \\ \phi \end{pmatrix} = \begin{pmatrix} R_{sl}[x - x_0(\sqrt{\epsilon}t)] \\ \Omega t + \phi_{sl}[x - x_0(\sqrt{\epsilon}t)] \end{pmatrix} + \sqrt{\epsilon}\chi(\epsilon^2 t) \begin{pmatrix} \rho_{as}(x - x_0) \\ \omega_{as}(x - x_0) \end{pmatrix} + \begin{pmatrix} 0 \\ \phi_0(\epsilon t) \end{pmatrix} + \epsilon^{5/2} \begin{pmatrix} P(x, x_0, \chi) \\ \Theta(x, x_0, \chi) \end{pmatrix}. \tag{39}$$

Using the same method of the previous section, and after straightforward calculations, we find the following amended reduced model

$$\dot{\chi} = g\chi + f\chi^3 + h\chi^5, \tag{40}$$

$$\dot{x}_0 = a\chi, \tag{41}$$

$$\dot{\phi}_0 = b\chi^2, \tag{42}$$

where

$$h = -\frac{\langle \psi_\varphi^{as} | \frac{\rho_{as}^5}{R_{ls}^5} \partial_{xx} R_{ls} \rangle}{\langle \psi_R^{as} | \rho_{as} \rangle + \langle \psi_\varphi^{as} | \omega_{as} \rangle} \tag{43}$$

is a negative coefficient. To carry out the above calculation, we assume that f is of order ϵ^2. Because the cubic coefficient is negative and small, and the quintic nonlinearity is negative and order one, the system presents a continuous supercritical bifurcation governed by the quintic term far from the bifurcation. The amplitude of the asymmetric mode now takes the form

$$\chi = \sqrt{\frac{f + \sqrt{f^2 + 4|h|g}}{|h|}}. \tag{44}$$

Then the amplitude of the symmetric mode increases with the bifurcation parameter as $\chi \sim (\Delta\mu)^{1/4}$. Likewise, the pulse speed increases with the power 1/4, $v = \dot{x}_0 \sim (\Delta\mu)^{1/4}$. Fig. 10a shows how the pulse speed follows a 1/4 power law. Note that the pulse speed is in excellent agreement with the previous prediction. On the other hand, the pulse frequency depends on χ^2, so the frequency increases with the square root of the bifurcation parameter $\dot{\phi}_0 \sim (\Delta\mu)^{1/2}$. Fig. 10b shows this behavior. The agreement, in this case, is not total due to the effect of the upper non-linear terms not considered in our approximation.

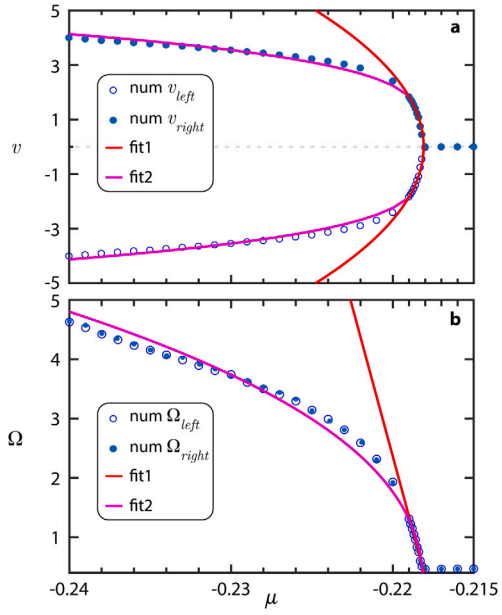

Fig. 10. Pulse speed and frequency as a function of bifurcation parameter of the Ginzburg–Landau model Eq. (15) with $d_r = 1.1$, $d_i = 0.7$, $\gamma_r = -1$, $\gamma_i = 0.5$, $\Delta x = 0.4$, and $\Delta t = 0.05$. (a) Pulse speed as a function of the bifurcation parameter μ. The circles account for the speed of the pulses obtained numerically. The red and purple curves account for the different power laws valid near ($v = 61.22\sqrt{-\mu - \mu_c}$ with $\mu_c = -0.2181$) and far ($v = \pm 10.74\sqrt[4]{-\mu - \mu_c}$) from the transition point. (b) Pulse frequency as a function of the bifurcation parameter. The circles account for the pulse frequencies obtained numerically from motionless and traveling pulses. The red and purple curves account for the different power laws valid near ($\dot{\phi}_0 = 1008(\mu_c - \mu) + \Omega_0$ and $\Omega_0 = 0.47$) and far ($\dot{\phi}_0 = 23(\mu_c - \mu)^{0.41} + \Omega_0$) from the transition point.

4. Laser dynamics close to lasing or oscillatory instability: class B lasers

The natural equilibrium of the set of Eqs. (1) is the non-lasing state $E = 0$, $G = A$, and $Q = B$, which corresponds to the quiescent state. This state exhibits a lasing or oscillatory instability, *Andronov–Hopf bifurcation*, for $A_c = B + 1$ with $\gamma > 0$ and a characteristic frequency $i(B\beta - \alpha A_c)$. To address the dynamical behaviors of this instability, we use the method of normal forms [57], which accounts for the evolution of the critical modes, *the central manifold*. Let us consider the ansatz

$$\begin{pmatrix} E \\ E^* \\ G \\ Q \end{pmatrix} = \begin{pmatrix} 0 \\ 0 \\ A_c \\ B \end{pmatrix} + C \begin{pmatrix} 1 \\ 0 \\ 0 \\ 0 \end{pmatrix} + C^* \begin{pmatrix} 0 \\ 1 \\ 0 \\ 0 \end{pmatrix} + |C|^2 \begin{pmatrix} 0 \\ 0 \\ -A_c \\ -B \end{pmatrix} + |C|^4 \begin{pmatrix} 0 \\ 0 \\ A_c + 2A_c \frac{(B(s-1)-1)}{\gamma} \\ Bs + 2B\frac{(B(s-1)-1)}{\gamma} \end{pmatrix} + h.o.t,$$

where $C = C(x,t)$ is the complex amplitude of the critical mode, C^* stands for the complex conjugate of C, and $h.o.t$ accounts for higher order terms in the amplitude C. Introducing the previous ansatz in the set of Eqs. (1), and after straightforward calculation, we get

$$\frac{\partial C}{\partial t} = \left(\mu' + d'|C|^2 + \Gamma|C|^4\right) C + i\frac{\partial^2 C}{\partial x^2}, \tag{45}$$

where

$$\mu' = \Delta + i[B\beta - \alpha A_c - \alpha\Delta], \tag{46}$$

$$\Delta = A - A_c = A - B - 1, \tag{47}$$

$$d' = B(s-1) - 1 + i\,[\alpha(B+1) - \beta B s]\,, \tag{48}$$

$$\Gamma = (B + 1 - Bs^2) - i[\alpha(B+1) - \beta B s^2] + + \frac{2(1 - B(s-1))}{\gamma}\,(B(s-1) - 1 + i\Omega)\,, \tag{49}$$

$$\Omega = \alpha A_c - \beta B s. \tag{50}$$

Note that Δ is the bifurcation parameter. Hence, the oscillatory bifurcation accounts for a subcritical instability described by the cubic–quintic Ginzburg–Landau equation (45), where $\mathrm{Re}\,(d') > 0$ and $\mathrm{Re}\,(\Gamma) < 0$. Therefore, as we show in Section 3, this model has a supercritical transition between motionless to traveling pulses. Unlike model (15), in this lasing instability, the coefficients of the amplitude equation depend on the recombination rates of non-radiative carriers γ. Note that in the adiabatic limit, $\gamma \to \infty$, we recover Eq. (15), but the amplitude equation (45) is valid also for finite γ, which accounts for class B semiconductor lasers.

5. Conclusion

We have studied theoretically and numerically the transition from traveling to motionless pulses in vertical-cavity semiconductor lasers with a saturable absorber. Numerically, we found that semiconductor lasers with saturable absorbers exhibit propagative and static pulses. However, experimental observations of this transmission have yet to be reported. To comprehend this transition, we have explored two different approaches. The first approach involves the adiabatic elimination of the charge carriers associated with a class A laser. The second approach involves analyzing the class B laser dynamics near the lasing instability. Indeed, in the adiabatic elimination limit, we consider large non-radiative carrier recombination rates. In this limit, we numerically have observed that the pulses exhibit a supercritical transition between traveling to motionless pulses. Using the asymptotic behavior of the pulse, we were able to set formulas for the pulse speed and frequency; both have an excellent agreement with the numerical findings. We have elucidated that the observed transition corresponds to the spontaneous breaking instability of reflection symmetry in the weak amplitude limit. We have established an equation for the pulse position, asymmetric amplitude, and frequency based on the reduction method. This model shows quite fair agreement with the numerical simulations for the different approaches considered for the semiconductor lasers with the saturable absorber. Close to the lasing instability, the system is described by the same equation as in the weak amplitude limit but with different parameters. Therefore, around this instability, the system also presents a supercritical transition from motionless to traveling pulses.

The adiabatic limit considered in the present work for the semiconductor laser with a saturable absorber is not realistic in experiments where excitable pulses have been observed since eliminating simultaneously the carries is impossible to achieve in lasers with good cavities. However, this limit allows a semi-analytical understanding of the properties of pulses and their respective instabilities. Note that near the lasing instability, the same type of pulses and transitions between them are expected to be observed.

Depending on the initial conditions, semiconductor lasers can exhibit multi-pulse solutions. It is also known that the Ginzburg–Landau equations display bound states of motionless pulses [58]. It is then expected that these bound states can also exhibit transitions from stationary bound states to traveling ones. Work on this type of transition and interaction of pulses is in progress. The possibility of using pulses excited and controlled by light opens the opportunity for new optoelectronic elements, which can be used as logic gates [59]. But to move in this direction, it is essential to understand the interaction of these pulses in the different regimes. Studies in this direction are in progress.

CRediT authorship contribution statement

F.R. Humire: Conceptualization, Investigation, Numerical simulations, Visualization, Writing – original draft. **K. Alfaro-Bittner:** Conceptualization, Investigation, Writing – review & editing. **M.G. Clerc:** Conceptualization, Formal analysis, Investigation, Visualization, Writing – review & editing. **R.G. Rojas:** Conceptualization, Investigation, Writing – review & editing.

Declaration of competing interest

The authors declare that they have no known competing financial interests or personal relationships that could have appeared to influence the work reported in this paper.

Data availability

No data was used for the research described in the article.

Acknowledgments

FRM-H acknowledges support from the Dirección general de investigación e innovación de la Universidad de Tarapacá, Arica, Chile, under the Proyecto UTA Mayor N° 4730-23. K. A.-B. acknowledges URJC Grants (Proyecto Impulso n° 2023/00004/001M2978). M.G.C. acknowledges the financial support of ANID-Millennium Science Initiative Program-ICN17_012 (MIRO) and FONDECYT project 1210353. R.G.R acknowledges DI Investigación Innovadora Interdisciplinaria PUCV 2021 N° 039.409/2021.

References

[1] J.D. Murray, Mathematical Biology II: Spatial Models and Biomedical Applications, Vol. 3, Springer New York, 2001.
[2] A. Scott, Neuroscience: A Mathematical Primer, Springer Science & Business Media, 2002.
[3] E.M. Izhikevich, Dynamical Systems in Neuroscience, MIT Press, 2007.
[4] W. Gerstner, W.M. Kistler, Spiking Neuron Models: Single Neurons, Populations, Plasticity, Cambridge University Press, 2002.
[5] M. Remoissenet, Waves Called Solitons: Concepts and Experiments, Springer Science & Business Media, 2013.
[6] C. Gu, Soliton Theory and Its Applications, Springer Science & Business Media, 2013.
[7] P.G. Drazin, R.S. Johnson, Solitons: An Introduction, Vol. 2, Cambridge University Press, 1989.
[8] A.C. Newell, Solitons in Mathematics and Physics, SIAM, 1985.
[9] F. Haudin, R.G. Rojas, U. Bortolozzo, M. Clerc, S. Residori, Vortex emission accompanies the advection of optical localized structures, Phys. Rev. Lett. 106 (6) (2011) 063901.
[10] B.-X. Li, R.-L. Xiao, S. Paladugu, S.V. Shiyanovskii, O.D. Lavrentovich, Three-dimensional solitary waves with electrically tunable direction of propagation in nematics, Nature Commun. 10 (1) (2019) 3749.
[11] J.K. Jang, M. Erkintalo, S.G. Murdoch, S. Coen, Ultraweak long-range interactions of solitons observed over astronomical distances, Nat. Photonics 7 (8) (2013) 657–663.
[12] S. Barland, O. Piro, M. Giudici, J.R. Tredicce, S. Balle, Experimental evidence of van der Pol–Fitzhugh–Nagumo dynamics in semiconductor optical amplifiers, Phys. Rev. E 68 (3) (2003) 036209.
[13] H. Bödeker, M. Röttger, A. Liehr, T. Frank, R. Friedrich, H.-G. Purwins, Noise-covered drift bifurcation of dissipative solitons in a planar gas-discharge system, Phys. Rev. E 67 (5) (2003) 056220.
[14] P. Coullet, Localized patterns and fronts in nonequilibrium systems, Int. J. Bifurcation Chaos 12 (11) (2002) 2445–2457.
[15] Y. Pomeau, Front motion, metastability and subcritical bifurcations in hydrodynamics, Physica D 23 (1–3) (1986) 3–11.
[16] V. Mendez, S. Fedotov, W. Horsthemke, Reaction-Transport Systems: Mesoscopic Foundations, Fronts, and Spatial Instabilities, Springer Science & Business Media, 2010.
[17] F.B. Jr, D.W. Bronk, M.G. Larrabee, Chemical excitation of nerve, Ann. New York Acad. Sci. 47 (4) (1946) 457–485.
[18] R. FitzHugh, Mathematical models of threshold phenomena in the nerve membrane, Bull. Math. Biophys. 17 (1955) 257–278.
[19] A.T. Winfree, The Geometry of Biological Time, Vol. 2, Springer, 1980.

[20] M. Tlidi, A. Vladimirov, D. Pieroux, D. Turaev, Spontaneous motion of cavity solitons induced by a delayed feedback, Phys. Rev. Lett. 103 (10) (2009) 103904.
[21] A. Alvarez-Socorro, M. Clerc, M. Tlidi, Spontaneous motion of localized structures induced by parity symmetry breaking transition, Chaos 28 (5) (2018) 053119.
[22] E. Bodenschatz, D.S. Cannell, J.R. de Bruyn, R. Ecke, Y.-C. Hu, K. Lerman, G. Ahlers, Experiments on three systems with non-variational aspects, Physica D 61 (1–4) (1992) 77–93.
[23] M.G. Clerc, S. Coulibaly, D. Laroze, Nonvariational Ising–Bloch transition in parametrically driven systems, Int. J. Bifurcation Chaos 19 (2009) 2717.
[24] M.G. Clerc, S. Coulibaly, D. Laroze, Localized states and non-variational Ising–Bloch transition of a parametrically driven easy-plane ferromagnetic wire, Physica D 239 (1–2) (2010) 72–86.
[25] F. Barra, O. Descalzi, E. Tirapegui, Nonvariational effects in nonequilibrium systems, Phys. Lett. A 221 (3–4) (1996) 193–196.
[26] P.R. Prucnal, B.J. Shastri, T.F. de Lima, M.A. Nahmias, A.N. Tait, Recent progress in semiconductor excitable lasers for photonic spike processing, Adv. Opt. Photonics 8 (2) (2016) 228–299.
[27] A.M. Yacomotti, M.C. Eguia, J. Aliaga, O.E. Martinez, G.B. Mindlin, A. Lipsich, Interspike time distribution in noise driven excitable systems, Phys. Rev. Lett. 83 (2) (1999) 292.
[28] S. Wieczorek, B. Krauskopf, D. Lenstra, Multipulse excitability in a semiconductor laser with optical injection, Phys. Rev. Lett. 88 (6) (2002) 063901.
[29] S. Barbay, R. Kuszelewicz, A.M. Yacomotti, Excitability in a semiconductor laser with saturable absorber, Opt. Lett. 36 (23) (2011) 4476–4478.
[30] B.J. Shastri, M.A. Nahmias, A.N. Tait, A.W. Rodriguez, B. Wu, P.R. Prucnal, Spike processing with a graphene excitable laser, Sci. Rep. 6 (1) (2016) 1–12.
[31] S. Barbay, R. Kuszelewicz, A.M. Yacomotti, Excitability in a semiconductor laser with saturable absorber, Opt. Lett. 36 (23) (2011) 4476–4478.
[32] M. Giudici, C. Green, G. Giacomelli, U. Nespolo, J. Tredicce, Andronov bifurcation and excitability in semiconductor lasers with optical feedback, Phys. Rev. E 55 (6) (1997) 6414.
[33] J.R. Tredicce, F.T. Arecchi, G.L. Lippi, G.P. Puccioni, Instabilities in lasers with an injected signal, J. Opt. Soc. Amer. B 2 (1985) 173.
[34] J. Ohtsubo, Semiconductor lasers, in: Stability, Instability and Chaos, Vol. 111, Springer, 2013.
[35] F. Selmi, S. Coulibaly, Z. Loghmari, I. Sagnes, G. Beaudoin, M.G. Clerc, S. Barbay, Spatiotemporal chaos induces extreme events in an extended microcavity laser, Phys. Rev. Lett. 116 (2016) 013901.
[36] S. Coulibaly, M.G. Clerc, F. Selmi, S. Barbay, Extreme events following bifurcation to spatiotemporal chaos in a spatially extended microcavity laser, Phys. Rev. A 95 (2017) 023816.
[37] S. Barbay, S. Coulibaly, M.G. Clerc, Alternation of defects and phase turbulence induces extreme events in an extended microcavity laser, Entropy 20 (2018) 789.
[38] G.P. Agrawal, N.K. Dutta, Semiconductor Lasers, Springer Science & Business Media, 2013.
[39] S.V. Fedorov, A.G. Vladimirov, G.V. Khodova, N.N. Rosanov, Effect of frequency detunings and finite relaxation rates on laser localized structures, Phys. Rev. E 61 (2000) 5814.
[40] N.N. Rosanov, Spatial Hysteresis and Optical Patterns, Springer Science & Business Media, 2002.
[41] M. Bache, F. Prati, G. Tissoni, R. Kheradmand, L.A. Lugiato, I. Protsenko, M. Brambilla, Cavity soliton laser based on VCSEL with saturable absorber, Appl. Phys. B 81 (2005) 913.
[42] F. Prati, G. Tissoni, L.A. Lugiato, K.M. Aghdami, M. Brambilla, Spontaneously moving solitons in a cavity soliton laser with circular section, Eur. Phys. J. D 59 (2010) 73.
[43] T. Schemmelmann, F. Tabbert, A. Pimenov, A.G. Vladimirov, S.V. Gurevich, Delayed feedback control of self-mobile cavity solitons in a wide-aperture laser with a saturable absorber, Chaos 27 (2017) 114304.
[44] S.V. Fedorov, N.N. Rozanov, A.N. Shatsev, Two-dimensional solitons in B-class lasers with saturable absorption, Opt. Spectrosc. 102 (2007) 449.
[45] P.A. Robinson, Nonlinear wave collapse and strong turbulence, Rev. Modern Phys. 69 (1997) 507.
[46] I.S. Aranson, L. Kramer, The world of the complex Ginzburg–Landau equation, Rev. Modern Phys. 74 (2002) 99.
[47] G. Baili, F. Bretenaker, M. Alouini, L. Morvan, D. Dolfi, I. Sagnes, Experimental investigation and analytical modeling of excess intensity noise in semiconductor class-A lasers, J. Lightwave Technol. 26 (2008) 952.
[48] G. Baili, L. Morvan, M. Alouini, D. Dolfi, F. Bretenaker, I. Sagnes, A. Garnache, Experimental demonstration of a tunable dual-frequency semiconductor laser free of relaxation oscillations, Opt. Lett. 34 (2009) 3421.
[49] C. Hessenius, N. Terry, M. Fallahi, J. Moloney, R. Bedford, Gain coupling of class A semiconductor lasers, Opt. Lett. 35 (2010) 3060.
[50] G. Baili, M. Alouini, T. Malherbe, D. Dolfi, I. Sagnes, F. Bretenaker, Direct observation of the class-b to class-A transition in the dynamical behavior of a semiconductor laser, Europhys. Lett. 87 (2009) 44005.
[51] H. Haken, Advanced Synergetics: Instability Hierarchies of Self-Organizing Systems and Devices, Vol. 20, Springer Science & Business Media, 2012.
[52] H. Sakaguchi, Motion of pulses and vortices in the cubic–quintic complex Ginzburg–Landau equation without viscosity, Physica D 210 (1–2) (2005) 138–148.
[53] V. Arnold, Chapitres supplémentaires de la théorie des équations différentielles ordinaires, MIR, Moscow, 1984.
[54] M. Clerc, P. Coullet, E. Tirapegui, Lorenz bifurcation: Instabilities in quasireversible systems, Phys. Rev. Lett. 83 (19) (1999) 3820.
[55] M. Clerc, P. Coullet, E. Tirapegui, The stationary instability in quasi-reversible systems and the Lorenz pendulum, Int. J. Bifurcation Chaos 11 (03) (2001) 591–603.
[56] L.M. Pismen, Patterns and Interfaces in Dissipative Dynamics, Vol. 30, Springer, 2006.
[57] C. Elphick, E. Tirapegui, M.E. Brachet, P. Coullet, G. Iooss, A simple global characterization for normal forms of singular vector fields, Physica D 29 (1987) 95–127.
[58] B.A. Malomed, Bound solitons in coupled nonlinear Schrödinger equations, Phys. Rev. A 45 (1992) R8321.
[59] V.A. Pammi, K. Alfaro-Bittner, M.G. Clerc, S. Barbay, Photonic computing with single and coupled spiking micropillar lasers, IEEE J. Sel. Top. Quantum Electron. 26 (1) (2019) 1–7.